(This is a preprint of an article to appear in the 1997 Ultrasonics Symposium Proceedings)

Studies of Broadband PMN Transducers Based on Nonlinear Models

G. Wojcik, J. Mould, D. Tennant, R. Richards†, H. Song, D. Vaughan, N. Abboud‡, D. Powell

Weidlinger Associates, 4410 El Camino Real, Los Altos, CA 94022
†Naval Undersea Warfare Center, 1176 Howell St., Newport, RI 02841
‡Weidlinger Associates, 375 Hudson Street, New York, NY 10014

Abstract — The Navy has an immediate need for large-scale, 3D, nonlinear simulations of broadband sonar projectors. The example considered here is a volume array of high-power, electrostrictive (PMN) flextensionals. Analysis and design of these complex arrays are clearly pushing the limits of simplified models. The analytical burden should be shifted from clever but overextended designers to computers. Very large-scale models, broadband response and nonlinearity favor explicit time-domain methods over implicit time- or frequency-domain methods. We demonstrate comprehensive finite element modeling of an icosahedral array of 12 electrostrictive flextensionals. Behavior of the PMN driver is illustrated with a 1D finite element (nonlinear harmonic oscillator) and generalized to a 3D element. Full-scale, SMP simulations are shown for individual flextensionals and the icosahedral array including tow-body structure.

Introduction

Virtually all sonar projectors used in operational Navy systems are driven by conventional PZT piezoceramics. However, it is clear that these drivers will not meet future naval needs, which include much higher power per unit volume and broadband capability. To achieve performance goals, efforts are underway utilizing electrostriction in lead magnesium niobate (PMN) to drive volume arrays of flextensionals. However, electrostriction is inherently nonlinear, i.e., strain is proportional to 2nd order polarization. These high-power flextensional arrays are currently designed and built on the basis of 1D, lumped parameter, linearized models. Although certainly useful and effective, this approach is at odds with the operational importance of 3D effects and the intrinsic nonlinearity of PMN. 3D structural and acoustic details along with material nonlinearity must be included in the design loop.

There are various analytical approaches available to the flextensional array designer, ranging from hybrid mathematical models to full numerical simulations. It is clear that much of the preliminary design can and should be done using existing, simplified models because of their speed and the veteran designer's facility with them. These linear models are used in combination with empirical data from a sequence of prototypes. However, as system requirements and active materials get more complex, it becomes increasingly difficult to make a coherent synthesis of the data and model parameters. The solution demonstrated here is to shift the burden to the computer, using comprehensive finite element models to reduce idealizations and provide a virtual prototyping capability. Virtual prototypes can, in principle, be used to focus on the critical details of array design, aid in experiment planning, and help explain the more arcane experimental results.

This paper demonstrates the scale of comprehensive computer modeling necessary to achieve useful virtual prototyping of 3D sonar arrays. Nonlinear material behavior, 3D flextensional response, and broadband acoustic interaction is included automatically in a time-domain finite element model of the array of flextensionals. In particular, we use the PZFlex finite element code [1] to model the 3D array of 12 flextensionals shown in Fig. 1. This array is based on the icosahedral design used in a collaboration between Lockheed Martin and the Naval Undersea Warfare Center (NUWC). Detailed 3D models

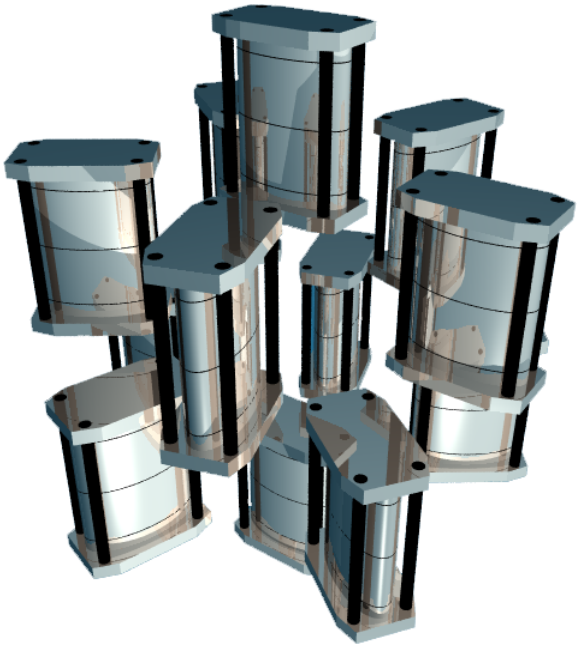

Fig. 1. The icosahedral array of 12 PMN-driven flextensionals (Lockheed Martin and NUWC collaboration).

of the flextensional and full volume array in a 2m x 2m x 2m cube of water with 10 kHz wave resolution require about 1 gigabyte of RAM. This size of simulation, which is readily done on a multi-processor workstation, includes complete nonlinear electromechanical interaction within each flextensional element and acoustic/mechanical interactions between them. The only operational difficulty is building the complicated 3D finite element model.

We also describe the time-domain electrostrictive simulation capability added to PZFlex. This is based on the simple constitutive model formulated by Hom and Shankar [2]. Electromechanical theory and behavior are illustrated succinctly by a 1D element (spring-mass model), although the capability in PZFlex is fully 3D. The principal numerical implementation issue is nonlinear dependence of polarization on electric field. Many, but not all, of the necessary constitutive properties of PMN have been measured by Winzer, et al. at Lockheed Martin, Powers and McLaughlin at NUWC, and Mukherjee and Sherrit at the Royal Military College of Canada.

Finite Element Modeling Issues

A 2nd order accurate explicit/implicit (mechanical/electrical), time-domain finite element algorithm [1] is used here for a number of compelling reasons. First, it maximizes problem size in given memory because the mechanical part scales linearly with the number of elements and the electrical system of equations is restricted to "windows" around the PMN. Second, it is ideal for broadband (transient) simulations, where both accuracy and stability dictate a small time step less than the Courant number for the grid. Third, nonlinearity is naturally modeled by an incremental approach, timestep by timestep. The fourth reason is that the algorithm is well-suited to parallel computing, which is essential at the problem scale required here.

In contrast to imaging arrays [1,3] that are mostly rectangular (Cartesian), the job of building finite element models of 3D sonar arrays like that in Fig. 1 is demanding. Using PZFlex, this consists of constructing the 3D physical structure and surrounding water with millions of "bricks" of the various passive and active materials. To this end it is essential that we be able to combine skewed and Cartesian grids for computational efficiency, and bond discontinuous meshes, e.g., a 5 to 1 size difference between water and transducer elements. Finite element size is dictated by wavelength in the water and by structural details in and around the transducers. Hexahedrons (bricks) are preferred over tetrahedrons because of lower cost and higher performance, i.e., relative anisotropic dispersion. Note that Cartesian elements are 1/5 the computational cost (floating point operations) of skewed elements.

To run these types of models it is vital that we accommodate disparate wavespeeds among different model regions, e.g., between elements of water ($v_L \approx 1500$ m/s) and aluminum ($v_L \approx 6380$ m/s) or PMN ($v_L \approx 4477$ m/s). The optimum timestep in each can differ by a factor of 50 because of relative wavespeed and element size. Therefore, subcycling is mandatory. This is simply a scheme for integrating neighboring elements or zones at their own near-optimal timestep, by making them integer multiples. Subcycling may be used, for example, to integrate 50 timesteps in a refined transducer mesh for each timestep in the surrounding coarse water mesh. Aggressive subcycling is required to maximize computer resources, making very large-scale problems feasible.

Coupled mechanical (hyperbolic) and electrical (elliptic) field calculations are required at each timestep and different algorithms are best for each. In particular, systems of nonlinear equations must be solved for the electric field in the PMN and the field is negligible outside because of PMN's very high relative dielectric constant. Therefore, the calculation can be confined to decoupled "electric windows," which may be solved in parallel, i.e., each assigned to its own processor. Details of the algorithm are described below.

Computer Requirements

Current and future array problems may require on the order of 50 million elements to capture the full range of physical scales and electromechanical interactions. No single central processing unit (CPU) is fast enough for reasonable turnaround. Furthermore, the entire calculation must be retained in random access memory (RAM) because disk I/O is still relatively slow. Therefore, multiple CPUs with large amounts of memory are necessary. We are currently using an 8-processor Silicon Graphics Origin 2000 server with 6 gigabytes of RAM.

There are essentially two multiple processor paradigms: parallel processing (PP) and symmetric multiprocessing (SMP). From our very focused perspective, PP splits the problem domain into pieces and assigns each to its own processor with dedicated memory, while SMP splits the range of each admissible do loop among the available processors with shared memory. PP runs a copy of the solver on each processor and requires message passing at internal boundaries using multiprocessing languages like PVM and MPI. SMP uses the multithreading paradigm and requires "index independence," i.e., no dependencies between different ranges in the do loop. PP is more scalable (two to thousands of processors) than SMP (two to tens of processors) because the later is limited by shared memory bandwidth. PP also requires significantly more code modifications. We utilize the SMP paradigm in the following because it is the basis for forthcoming multiprocessor platforms using inexpensive personal computer technology.

Electrostrictive Modeling

In electrostrictive materials, an applied electric field E produces strain S_P proportional to second order polarization P, i.e., $S_P = QP^2$ in 1D, where Q is the electrostrictive coefficient. A number of constitutive theories exist for electrostrictors, e.g., [4,5]. An attractive phenomenological theory was proposed recently by Hom and Shankar [2]. They use the approach of Suo [4] and add an explicit formula for polarization saturation that appears more natural than polynomial assumptions, e.g., [5]. From a formula used in [6] to model piezoelectric hysteresis, the satura-

tion model assumed for polarization at zero stress is

$$P = P_S \tanh(\kappa E) \quad \Rightarrow \quad E = \frac{1}{\kappa}\tanh^{-1}\left(\frac{P}{P_S}\right) \qquad (1)$$

where P_S is spontaneous (or saturation) polarization and κ is a material constant. Note that electric displacement $D=\varepsilon_0 E+P$, so from (1) $D=\varepsilon_0 E+P_S\tanh(\kappa E)\approx\varepsilon_0 E+P_S\kappa E$ for small E and zero stress. Since $P_S\approx 0.259$ C/m^2 and $\kappa\approx 1.16\text{x}10^{-6}$ m/V in the PMN considered here [2], free-space permittivity $\varepsilon_0=8.854\text{x}10^{-12}$ C/V/m is negligible compared to $P_S\kappa\approx 0.3\text{x}10^{-6}$ C/V/m, i.e., relative permittivity $\varepsilon=P_S\kappa/\varepsilon_0\approx 34{,}000$. Therefore, electric displacement is effectively equal to polarization, $D\approx P$, for small E and zero stress. In 1D the Hom and Shankar continuum constitutive relations become

$$T = cS_M - cQP^2 \quad , \quad E = -2QTP + \frac{1}{\kappa}\tanh^{-1}\left(\frac{P}{P_S}\right) \qquad (2)$$

where T is stress, S_M is elastic strain, c is elastic stiffness, and temperature dependence is neglected.

We first consider the simplest electrostrictive spring-mass model of a PMN bar with area A, length L, and density ρ. This lumped mass ($m=\rho AL/2$) approximation pictured at the top of Fig. 2 constitutes the basic 1D finite element. Multiplying stress by area A and electric field by length L in (2) yields the spring constitutive equations as

$$F = -ku + kLQP^2 \quad , \quad V = \frac{2LQ}{A}FP + \frac{L}{\kappa}\tanh^{-1}\left(\frac{P}{P_S}\right) \qquad (3)$$

where $F=-AT$ is spring force, $k=AC/L$ is spring stiffness, $u=u_1-u_2=LS_M$ is spring compression, and $V=LE$ is voltage. Differentiating the voltage equation in (3) with respect to time and solving for dP/dt yields

$$\dot{P} = \frac{\left(\dot{V}+2(LQ/A)kP\dot{u}\right)\left(P_S^2-P^2\right)}{(LP_S/\kappa)+2(LQ/A)k\left(-u+3LQP^2\right)\left(P_S^2-P^2\right)} \equiv \frac{I}{A} \qquad (4)$$

where overdots denote time derivatives. I is electric current, equal to the time derivative of electric displacement $D\approx P$.

To write the governing ordinary differential equations (ODEs), assume symmetric response so that $u_1=-u_2=u/2$, set F in (3) equal to mass times acceleration, $(m/2)d^2u/dt^2$, and use (4) to write

$$\frac{d}{dt}\begin{pmatrix} u \\ \dot{u} \\ P \end{pmatrix} = \begin{pmatrix} \dot{u} \\ 2F/m \\ I/A \end{pmatrix}. \qquad (5)$$

Initial conditions are calculated from (3) by prescribing bias voltage V_B and "prestress" F_0 (with zero bias voltage) and solving the static nonlinear equations (using Newton's method, for example) for "bias polarization" P_B and "precompression" u_0. We assume zero initial velocity. The system of equations in (5) is solved using standard ODE solvers, e.g., 4th order Runge-Kutta.

An example of electrostrictive oscillator response is shown in Fig. 2. Dimensions of the bar are equal to the PMN multilayer stack used in the flextensional (see below). Bias voltage is centered in the linear part of the static displacement-voltage curve as shown. Applied voltage is sinusoidal and ramped up over seven cycles. At low drive voltages the response is essentially sinusoidal but as voltage is increased, harmonic distortion appears due to the nonlinear constitutive behavior. Fig. 2 shows the distorted velocity waveform and its amplitude spectrum when applied voltage is 66% of the bias voltage. Numerical experiments indicate that the higher harmonics generated are particularly sensitive to damping.

The 3D electrostrictive finite element algorithm is more involved but conceptually similar to the 1D algorithm developed and demonstrated above. It will not be described here. Suffice it to say that the electrostrictive algorithm

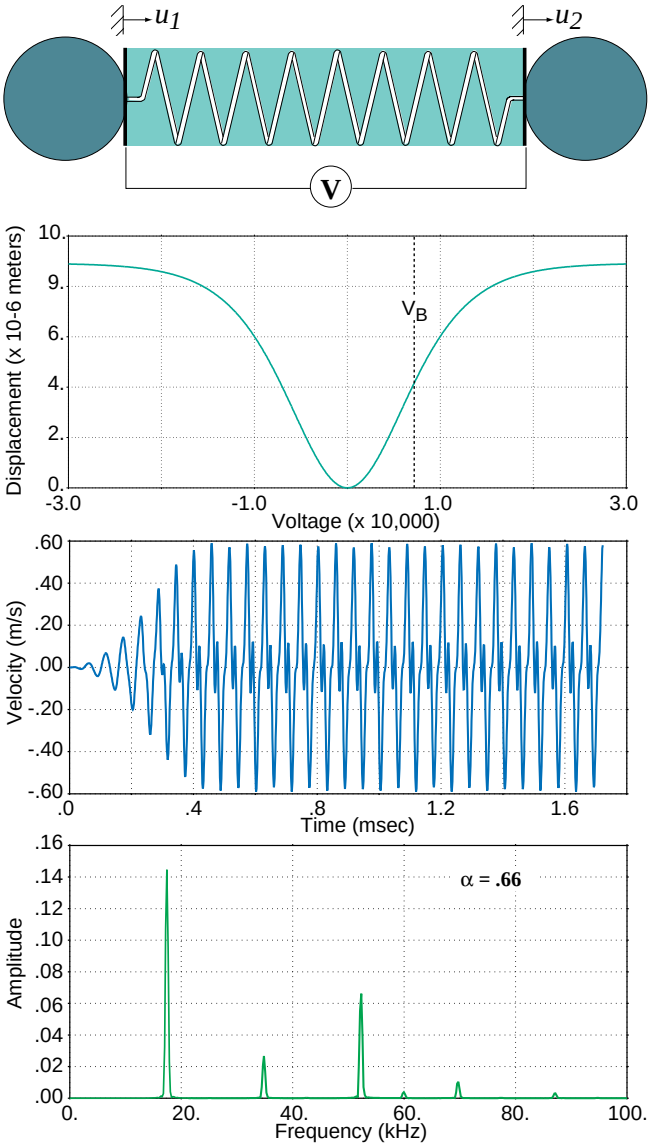

Fig. 2. Nonlinear behavior of the PMN harmonic oscillator model, showing static displacement versus voltage (top), velocity response to a 17.5 kHz sine wave at 66% of the bias voltage V_B (middle) and the spectrum quantifying harmonic generation (bottom).

consists of the standard electromechanical algorithm in PZFlex plus the nonlinear electric field solver for P, u, and E. This solver uses a Newton iteration with constant matrix based on the initial value of dP/dE, and an interior Newton iteration to solve the transcendental equation for P at fixed strain.

Flextensional Simulations

The first level of 3D model complexity we considered was the single electrostrictive flextensional in water. This model was driven with a transient, 1 kV voltage pulse on a 4 kV bias with prestress sufficient to keep the PMN driver in compression. The simulation ran until electrical response reached zero asymptotically, i.e., through its "ringdown" phase as acoustic waves radiated the flextensional's energy into the surrounding water. Time histories of voltage and current were Fourier transformed and impedance or admittance versus frequency calculated. The conductance plot (real part of admittance) is shown in Fig. 3. Note that 4.5 kHz is the design frequency for this device and model discretization provides adequate resolution out to 9 kHz. Also in Fig. 3 is a model cross-section showing the acoustic wave pattern at 4.5 kHz. Water boundaries are terminated with a local radiation condition, which is seen to be quite effective. At this design frequency, the radiation pattern is nearly omnidirectional.

Magnified modal response is illustrated by a cutaway and cross-sections in Fig. 4 at the 4.5 kHz driving frequency. The cutaway shows details of the flextensional model, consisting of two 10-layered PMN stacks, .35 x 1.5 x 2.1 in., with cofired electrodes and capped with prestress shims. These drive two elliptical rings or thick shells (flextensionals) between endplates held together by four Delrin/aluminum tension rods. In practice, Teflon contacts are used to reduce friction at the endplate-ring interface, so sliding on the contact surface is modeled with a Coulomb friction interface element. Note that a parameter study showed minor performance dependence on low to moderate friction angles.

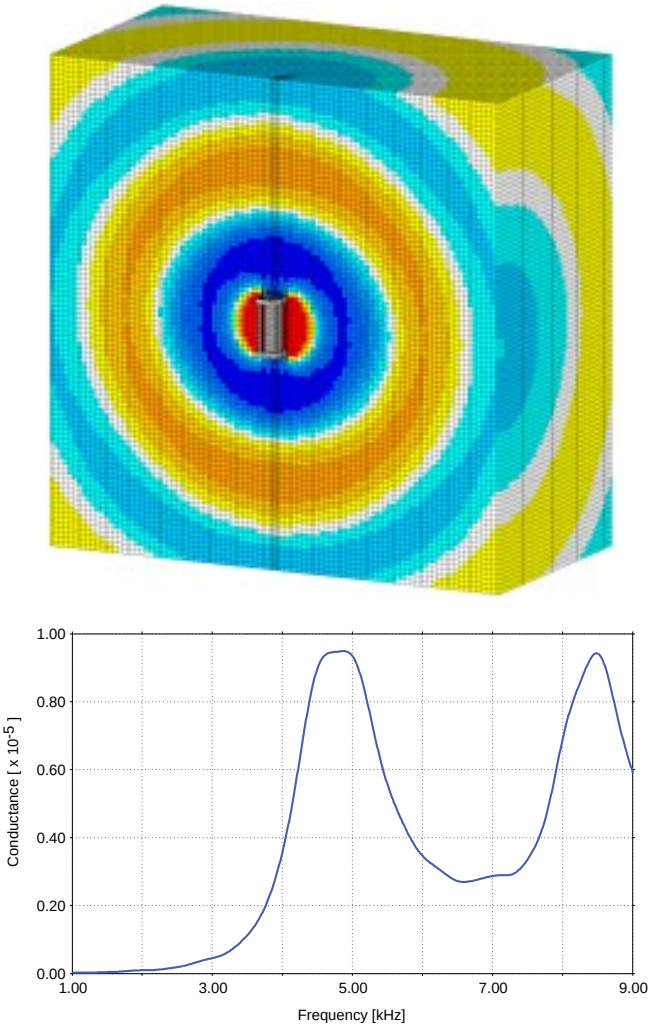

Fig. 3. Behavior of a single flextensional model driven in water, showing wave pattern and electrical response.

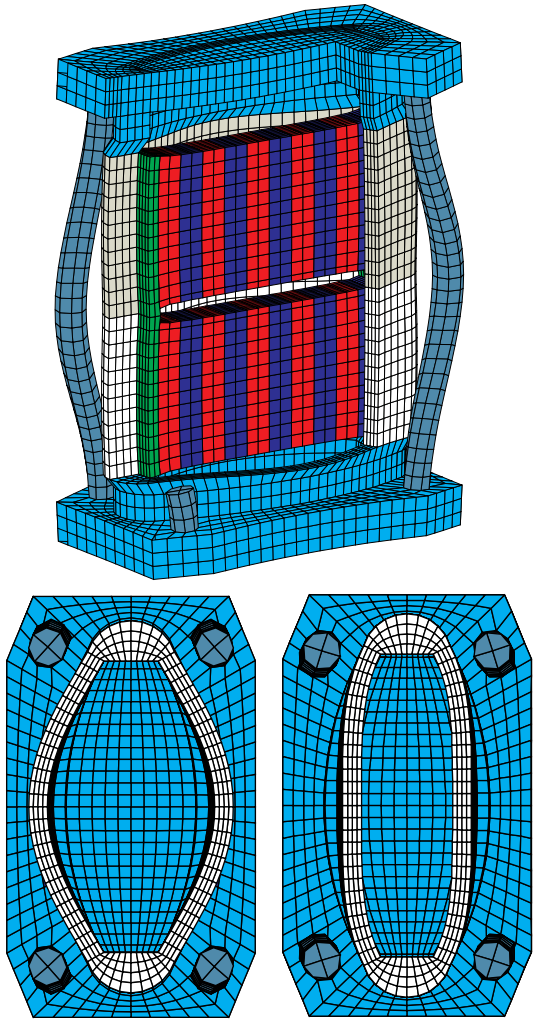

Fig. 4. Views of mode shapes in the single flextensional model driven at 4.5 kHz.

Both 1D and 3D drivers were used in the flextensional simulations. The 3D model is in the cutaway in Fig. 4, while the 1D model from Fig. 2 drove the ring deformation cross-sections of Fig. 4. At operational frequencies around 4.5 kHz, flextensional acoustic performance was essentially independent of 1D or 3D driver details, although not at higher frequencies, specifically, the 8.5 kHz mode. However, despite low frequency acoustic equivalence, important 3D stack response details are observed. In particular, Poisson effects cause high shear strain in the outer PMN layers of each stack. This deformation is seen in Fig. 4 and correlates with a number of experimental stack failures observed in the outer PMN layer. Note that tension rod oscillations shown in Fig. 4 can be complex and are, of course, sensitive to cross-section and end details.

Array Simulations

The next level of 3D model complexity was the icosahedral array of flextensionals in a 2x2x2 m^3 box of 1 cm^3 water elements, terminated by radiation conditions. A blowup of the model is shown in Fig. 5, where water elements in the top half are made transparent. This calculation used the 1D PMN drivers in each flextentional. The principal difficulty with models of this complexity is bonding the various meshed regions, e.g., connecting the skewed and very detailed flextensional array mesh to the trivial Cartesian water mesh. To save time building the model we simply voided overlapping elements in the array mesh, trading redundant computation and memory for setup time. There are a number of similar modeling tradeoffs, most of which can be removed by programming more efficient, tailored modeling constructs.

The array was phased to project a beam towards the upper left in Fig. 5 and driven by a 4.5 kHz, 1 kV peak-to-peak sine wave on a 4 kV bias, with prestress. A snapshot of the radiated acoustic field is shown in Fig. 6 on a vertical (symmetric) exposure through the cube of water. The beam pattern measured from this calculation is very close to experimental observations. Besides showing uniformity of the calculated wave field and effectiveness of the radiation boundary conditions, this view confirms that time-domain analysis is able to capture relatively low frequency flextensional array response. Array diameter is comparable to wavelength, which is much larger than structural details of the flextensionals. Nonetheless, the full range of length scales is represented by the calculation. Note that the subcycling ratio was 50 in this case, i.e., 50 timesteps in the array mesh for each timestep in the water mesh.

The last level of model complexity considered was the icosahedral array model in a fiberglass box representing a rudimentary tow-body with a steel strongback (mount) above and a lead ballast plate below. This is pictured in Fig. 7. The flextensional model is identical to the previous case, Fig. 5, but with material properties redefined in water elements coinciding with the tow-body structure. Results from this calculation are shown in Fig. 8. The point is that with the level of discretization available, the volume array and surrounding structure can be included in "production" finite element models of sonar projectors and similar devices.

These large-scale array models use approximately 10 million elastic finite elements, run in single-precision (32 bit word), and require about one GByte of random access memory. For these and similar calculations, parallel efficiency on an 8-processor SGI Origin 2000 SMP machine is 70%, i.e., the effective processor count is 0.7x8=5.6. On a single processor these calculations take ≈150 hours, but only 27 hours in SMP mode. Note, however, that if we had used the 3D PMN driver, run time would have increased significantly.

Discussion and Conclusions

We have developed an electrostrictive finite element modeling capability. It is fully operational within PZFlex, an explicit, time-domain, electromechanical code for large-scale structural dynamics and wave propagation. Pertinent finite element modeling issues are discussed and multiple processor computing is reviewed, emphasizing

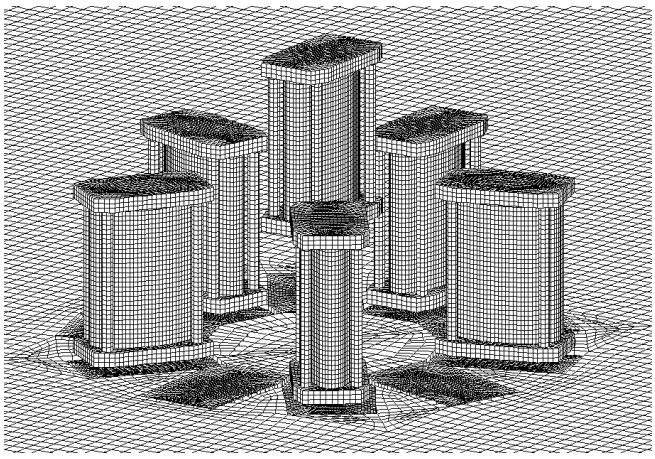

Fig. 5. View of the finite element model showing upper half of array and lower half of 2m x 2m x 2m water cube.

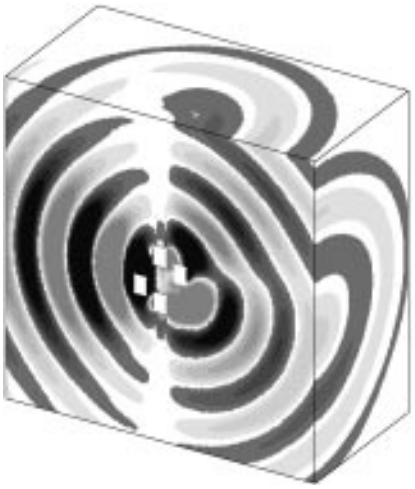

Fig. 6. Radiated acoustic field in the icosahedral array model. Phasing projects a beam to the left.

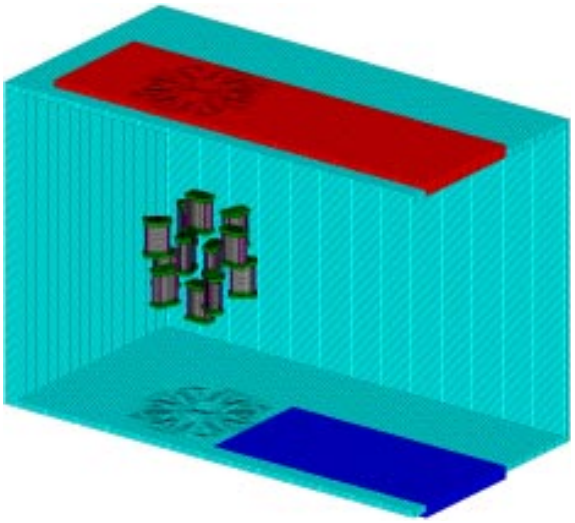

Fig. 7. PZFlex finite element model of icosahedral array within a fiberglass box with steel strongback and lead ballast plate.

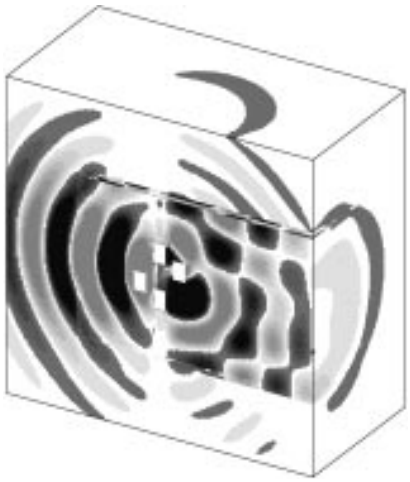

Fig. 8. Radiated accoustic field from the icosahedral array in a fiberglass box with a strongback and ballast plate.

the symmetric multiprocessing (SMP) paradigm. The 3D electrostrictive algorithm is based on the constitutive model proposed in [2], and demonstrated for a nonlinear harmonic oscillator corresponding to the simplest 1D finite element. Models of the flextensional and array designs by Lockheed Martin are built and large-scale simulations run on an SMP machine with 8 processors.

These calculations prove the utility of the explicit, time-domain algorithm for low-frequency sonar-type problems. Until now, sonar problems have been solved almost exclusively using implicit methods. Furthermore, we have demonstrated the ability to simulate the entire range of relevant length scales in production calculations that run in a reasonable amount of time on available multiprocessor workstations. The flextensional and bare array simulations described here were actually much larger than required. The absorbing boundary condition is effective enough to permit halving the model in each direction, yielding a problem 1/8 the original size. However, the array and "tow-body" combination do require the problem scale demonstrated. Note that steady state or transient beam patterns may be calculated by the Kirchhoff integral of pressure and velocity time histories on a nodal box surrounding the flextensional or array.

All of our initial modeling objectives have been met in this exercise by adding electrostrictive finite elements (1D, 2D, 3D) to PZFlex and modifying its core code loops for the SMP paradigm. The next set of objectives must include model and code validations against laboratory and field tests at the material, flextensional, and array levels. For example, the fundamental PMN constitutive model [2] has not been validated against any resonator (dynamic) data at this time, irrespective of finite element modeling issues. Clearly, PMN resonator validations must be the first order of business. These should be followed by finite element model validations against existing electrical and acoustic data from the flextensional, which would naturally lead to validations against array data.

This exercise also suggests various modeling enhancements, including model building (software) tools, useful GUI constructs, hysteresis models, and coupled thermal capability. All of these enhancements have been developed by us in one form or another. They simply have to be extended and/or incorporated in the production code. Nonetheless, the capability for large-scale, 3D, nonlinear simulations of broadband, electrostrictive, flextensional arrays is now available, in production mode, for parameter studies and design iterations of potentially useful sonar projector systems.

Acknowledgements

This work was supported by the Office of Naval Research and monitored by Mr. Scott Littlefield and Dr. Wallace Smith.

References

[1] G. Wojcik, D. Vaughan, N. Abboud, J. Mould, "Electromechanical modeling using explicit time-domain finite elements," *Proc. IEEE Ultrason. Symp.*, **2**, 1107-1112, 1993.

[2] C. Hom and N. Shankar, "A fully coupled constitutive model for electrostrictive ceramic materials," *Journal of Intelligent Material Systems and Structures*, vol. 5, 795-800, 1994.

[3] G. Wojcik, D. Vaughan, V. Murray, J. Mould, "Time-domain modeling of ultrasonic arrays for underwater imaging," *Proc. IEEE Ultrason. Symp.*, **2**, 1027-1032, 1994.

[4] Z. Suo, "Mechanical concepts for failure in ferroelectric ceramics," *Smart Structures and Materials*, ASME, AD Vol. 24/AMD Vol. 123, 1-6, 1991.

[5] K. Uchino, S. Nomura, L. Cross, R. Newnham, S. Jang, "Electrostrictive effect in perovskites and its transducer applications," *Journal of Materials Science*, vol. 16, 569-578, 1981

[6] X. Zhang and C. Rogers, "A macroscopic phenomenological formulation for coupled electromechanical effects in piezoelectricity," *Journal of Intelligent Material Systems and Structures*, vol. 4, 307-316, 1993.